

Identification of novel molecular candidates for fatty liver in the hyperlipidemic mouse model, HcB19

Marleen M. J. van Greevenbroek,¹ Vicky M. M.-J. Vermeulen, and Tjerk W. A. de Bruin

Laboratory of Molecular Metabolism and Endocrinology, Cardiovascular Research Institute Maastricht (Carim), and Department of Internal Medicine, Maastricht University, UNS 50/Box 14, P.O. Box 616, 6200 MD Maastricht, The Netherlands

Abstract The inbred HcB19 mouse strain expresses a truncated form of thioredoxin interacting protein and is phenotypically characterized by fatty liver and elevated plasma triglycerides and VLDL. Recently, these mice have been proposed as an animal model for familial combined hyperlipidemia. The aim of the present study was identification of hepatic proteins specifically associated with the presence of fatty liver. Eighteen differential proteins were detected in whole-liver homogenate from HcB19, or the parental strain C3H, using 2D electrophoresis, and 11 of those were successfully identified by mass spectrometry. Five of the identified differential proteins were mitochondrial, two peroxisomal, two cytosolic, and two secretory. Four differential proteins were novel in the fatty liver proteome [i.e., aconitase, succinate dehydrogenase, propionyl CoA carboxylase α chain (PCCA), and 3-hydroxyanthranilate 3,4 dioxxygenase (3HAAO)]. Of these, PCCA and 3HAAO are of particular interest because of their known functions in nicotinic acid metabolism (3HAAO) and ketogenesis (PCCA). We have newly identified several differential proteins in the hepatic proteome of mice with fatty liver, including PCCA and 3HAAO, and confirmed differential expression of previously reported proteins. These individual proteins, PCCA and 3HAAO, can be important in development of fatty liver or in the expression of hyperlipidemia.—van Greevenbroek, M. M. J., V. M. M.-J. Vermeulen, and T. W. A. de Bruin. **Identification of novel molecular candidates for fatty liver in the hyperlipidemic mouse model, HcB19.** *J. Lipid Res.* 2004. 45: 1148–1154.

Supplementary key words 3-hydroxyanthranilate 3,4 dioxxygenase • propionyl CoA carboxylase α chain • proteomics • steatosis • thioredoxin • thioredoxin interacting protein

Fatty liver, also known as hepatic steatosis or nonalcoholic steatohepatitis (NASH), is characterized by the accumulation of fat droplets within the cytoplasm of hepatocytes (1). Two essentially different metabolic processes can underlie the development of fatty liver. First, hepatic triglycerides (TGs) may accumulate because of an inade-

quate capacity of the liver to secrete TGs in VLDL. This has been reported in human subjects with hypobetalipoproteinemia (2). Second, TG synthesis in the liver may be accelerated to such an extent that mechanisms for fat oxidation and secretion are no longer sufficient to prevent intrahepatic TG accumulation. In this latter case, fatty liver can be associated with increased rates of VLDL secretion [as reviewed in ref. (3)]. An example is fatty liver in human subjects with familial combined hyperlipidemia (FCHL) (4), as well as type 2 diabetes mellitus and the metabolic syndrome [as reviewed in ref. (5)].

In general, fatty liver is a benign condition, but it can potentially progress into NASH, with the risk of progression into end-stage liver disease, i.e., cirrhosis or hepatocellular carcinoma (6, 7). Current literature suggests that progression from fatty liver to steatohepatitis may occur by a two-step mechanism in which insulin resistance may comprise the initial step (8), and the second step may be through oxidative damage. Furthermore, steatosis or NASH also contributes to, or reflects, insulin resistance of the liver, thus promoting a vicious circle of increasing insulin resistance and steatosis (3). Proteins induced in these mechanisms may be of great importance in advancing understanding of these processes, or even be potential therapeutic targets. To our knowledge, only a few studies addressed protein expression in NASH (9–11).

Abbreviations: 3HAAO, 3-hydroxyanthranilate 3,4 dioxxygenase; ACO2, aconitase; ALB, albumin; ATP5B, ATP synthase β chain; ATP5H, ATP synthase D chain; BiP, binding protein; CAT, catalase; CPS1, carbamoyl-phosphate synthase 1; ER, endoplasmic reticulum; FCHL, familial combined hyperlipidemia; FTCD, formiminotransferase cyclodeaminase; HPCL2, 2 hydroxy phytanol CoA lyase; HSPA9, heat shock protein 70 kDa protein 9; HSPA5, glucose-regulated 78 kDa protein; IEF, isoelectric focusing; MALDI-TOF, matrix-assisted laser desorption/ionization-time of flight; MW, molecular weights; NASH, nonalcoholic steatohepatitis; PCCA, propionyl CoA carboxylase α chain; PRDX, peroxiredoxin; SDHA, succinate dehydrogenase subunit A; TCA, trichloroacetic acid; TF, transferrin; TG, triglyceride; TRX, thioredoxin; TXNIP, thioredoxin interacting protein.

¹ To whom correspondence should be addressed.
e-mail: m.vangreevenbroek@intmed.unimaas.nl

Manuscript received 17 February 2004.

Published, JLR Papers in Press, April 1, 2004.
DOI 10.1194/jlr.M400062JLR200

The HcB19 mouse strain is an inbred mouse strain on a C3H background. HcB19 mice are phenotypically characterized by hyperlipidemia, elevated plasma levels of apolipoprotein B, and free fatty acids, as well as hypersecretion of hepatic TGs and increased hepatic TG levels (12). Recently, the gene defect in HcB19 was identified in thioredoxin interacting protein (TXNIP) (13). The TXNIP gene encodes a cytoplasmic inhibitor of thioredoxin (TRX), a major regulator of cellular redox state. These mice have been proposed with a hepatic fatty acid metabolism defect, channeling fatty acids toward ketogenesis (13). Interestingly, TXNIP has a chromosomal location that is syntenic with human chromosome 1q21-23, a locus that showed linkage with FCHL in several populations (14–16), although the contribution of TXNIP to FCHL is still unknown. The HcB19 mouse thus represents an animal model of fatty liver in combination with elevated plasma TGs, caused at least in part by VLDL overproduction. It shares many features with the metabolic syndrome and also with FCHL, especially with those patients that express combined hyperlipidemia or isolated hypertriglyceridemia. It was the aim of this study to identify differentially-expressed proteins in livers of HcB19 mice versus the parental C3H strain, to improve our insight into the metabolic pathways that contribute to development of fatty liver in hyperlipidemia, and to advance insights into the role of the TXNIP/TRX system in this process.

MATERIALS AND METHODS

Collection of plasma and liver

HcB19 mice and C3H mice (courteous gift of P. Demant) were maintained at the laboratory animal facility of the Maastricht University at a 12 h day/night cycle on normal dietary chow. Prior to the collection of plasma and tissue, mice were fasted overnight in a clean cage. Blood was collected via orbital puncture in gel tubes (microtainer SST, Becton and Dickinson) containing 10 μ l of 660 mM EDTA on ice. The animals were sacrificed after blood collection, the liver was excised, rinsed in ice-cold saline, snap-frozen in liquid N₂, and stored in liquid N₂. For each animal, the total procedure of blood and liver sampling was completed in less than 15 min. Blood samples in EDTA were centrifuged (5 min at 13,000 rpm, 4°C), and the plasma fraction was transferred into new tubes and immediately frozen at –20°C. All procedures were approved by the Animal Ethical Committee of the University of Maastricht.

Biochemical procedures

Plasma cholesterol, TGs, and NEFA were determined colorimetrically (Roche Diagnostics, Germany). Total iron was determined in liver homogenates (17). Protein concentrations were determined using the BioRad protein assay (BioRad, The Netherlands).

2D electrophoresis

Liver tissue was homogenized in isoelectric focusing (IEF) sample buffer [9.5 M urea, 2% (w/v) CHAPS, 0.8% (w/v) Pharylate pH 3–10, 1% (w/v) DTT] to a final concentration of 2–10 mg/ml. As protease inhibitor, complete protease inhibitor cocktail tablets (Roche) were used according to manufacturer's description. Isoelectrofocusing was performed on an IPGPhor

(Amersham-Pharmacia) using 3–10 linear 18 cm IPG strips (Immobiline Dry Strips, Amersham-Pharmacia). A sample (75 μ g) was loaded and active rehydration was performed for 16 h at 30 V and 20°C. IEF strips were run at 100 V (1 h), 150 V (1 h), 200 V (1 h), 500 V (1 h), 1,000 V (1 h) gradient to 8,000 V in 390 min, and 8,000 V (3 h), and were subsequently stored at –80°C until the second run was performed. Prior to the second run, IPG strips were equilibrated for 15 min in 6 M urea, 30% w/v glycerol, 2% SDS, and 1% (w/v) DTT, and then in 6 M urea, 30% w/v glycerol, 2% SDS, and 4% (w/v) iodoacetamide, respectively. IPG strips were loaded on 10% polyacrylamide gels (18.5 cm \times 20 cm), and a piece of filterpaper soaked with 15 μ l of protein standard (BioRad) was run at the side of the gels for reference of molecular weights (MW). Gels were sealed with low-melt agarose and run for 8 h at 200 V in a Dodeca Cell (BioRad). Gels were fixed in 50% methanol and 5% glacial acetic acid for 1 h at room temperature and silver-stained according to the mass spectrometry-compatible method adapted from Shevchenko (18). Gels were stored in milliQ water at 4°C until spot excision.

Gel images were captured with an 800 GS scanner (BioRad) and analyzed using PDquest software (BioRad). Protein spots were quantified after normalization for total protein on the gel. Liver homogenates from three HcB19 mice and three C3H mice were each analyzed in triplicate on 2D gels, so a total of 18 gels were used in the analyses. For statistical analyses, the average results of the triplicates were calculated, and the resulting values were used as independent data-points in statistical analyses. Spots with $P < 0.1$ were manually excised. An exception to this approach was made for a series of proteins at the top of the 2D gels (>100 kDa) that were clearly present in C3H and less so in HcB19. Considerable distortion in this part of the gels hindered the use of reliable landmarks, making analysis with the PDquest software not feasible. Therefore, this series of spots were quantified using Quantity One software (BioRad). Statistical analysis of these data was done exactly as described for the PDquest data.

In-gel digestion

Generally, protein spots to be identified were picked from 5–8 different gels and pooled prior to in-gel digestion. Protein spots were manually excised from the gel and processed on a MassPREP digestion robot (Waters, Manchester, UK) according to the following protocol: silver-stained spots were destained with 15 mM potassium ferricyanide/50 mM sodium thiosulphate. Disulfide bonds were reduced with 10 mM DTT in 100 mM ammonium bicarbonate for 30 min, followed by alkylation with 55 mM iodoacetamide in 100 mM ammonium bicarbonate for 20 min. Spots were washed with 100 mM ammonium bicarbonate to remove excess reagents and dehydrated with 100% acetonitrile. Trypsin (6 ng/ μ l) in 50 mM ammonium bicarbonate was added to the gel plug and incubated at 37°C for 5 h. The peptides were extracted with 1% formic acid/2% acetonitrile.

Mass spectrometry

For matrix-assisted laser desorption/ionization-time of flight (MALDI-TOF) mass spectrometry, 1.5 μ l of each peptide mixture and 0.5 μ l matrix solution (10 mg/ml α -cyano-4-hydroxycinnamic acid in 50% acetonitrile/0.1% trifluoroacetic acid) was spotted automatically onto a 96-well-format target plate. The spots were allowed to air dry for homogenous crystallization. Spectra were obtained using a MALDI-linear reflectron mass spectrometer (Waters, Manchester, UK). The instrument was operated in positive reflectron mode. Acquisition mass range was 900–3,000 Da. The instrument was calibrated on 6–8 reference masses from a tryptic digest of alcohol dehydrogenase. In addition, a nearpoint lockmass correction for each sample spot was performed using adrenocorticotropin 1–39 (MH+ 2,465.199) to

achieve maximum mass accuracy. Typically, 100 shots were combined, background subtracted, slightly smoothed, centroided, and deisotoped. A peptide mass list was generated for subsequent database search. MALDI procedures were done in the Maastricht Proteomics Center. When peptide masses in the spectra were low, samples were concentrated on zip-tips (Millipore) and rerun. Protein spectra were identified in the MASCOT program (<http://www.matrixscience.com>, Matrix Science Ltd.). One miscleavage was tolerated, and carbamidomethylation was set as a fixed modification. The proteins with a significant MOWSE score were checked for their (calculated) MW. Protein identifications were considered correct when this (calculated) MW agreed with the mass of the spot on the 2D gels.

Confirmation of proteome analysis results

The MALDI results for catalase (CAT) were confirmed on Western blotting. Equal amounts of liver homogenate were separated on 7.5% SDS-PAGE and transferred to polyvinylidene difluoride membrane. Membranes were probed with antiCAT (polyclonal antiCAT, SanverTech) and a peroxidase-conjugated secondary antibody (anti-rabbit, SanverTech) and developed by enhanced chemoluminescence (Pierce SuperSignal, West Pico). The image was captured with a FluorS imager (BioRad) and analyzed using the Quantity One software. Likewise, MALDI results for succinate dehydrogenase (SDH) were confirmed using anti-70 kDa SDH flavoprotein (molecular probes) and a peroxidase-conjugated secondary antibody (anti-mouse, Dako). The results for peroxiredoxin 1 (PRDX1) were confirmed using RT-PCR with the housekeeping gene β -actin as a reference. Total cDNA was prepared using a Superscript first-strand synthesis system for RT-PCR (Invitrogen) according to the manufacturer's instructions. A duplex PCR was performed using the following primers: PRDX upper ATGTCTTCAGGAAATGCAAAAATT, PRDX lower TCACTTCTGCTTAGAGAAATACTCT (600 bp PCR product), β -actin upper TCTTTGATGTCACGCACGATTTTC, and β -actin lower ATCGTGGGCCGCTCTAGGCACC (202 bp PCR product). Runs were performed at 60°C for 20 and 22 cycles, which was within the linear range of the amplification, and PCR products were separated on 1.5% agarose gel. The image was captured with a FluorS imager and analyzed using the Quantity One software.

Statistical analyses

Data are given as mean \pm SD. Data for plasma TG as well as hepatic TG and iron contents were analyzed after log transformation because their nontransformed distributions were skewed. Differences for means were calculated with Student's *t*-test using the SPSS analysis package (version 9.0). Significance was defined as $P < 0.05$.

RESULTS

Biochemical phenotype

HcB19 mice had significantly higher plasma levels of TG, cholesterol, and NEFAs than C3H mice (Table 1). The livers of HcB19 mice were steatotic compared with C3H. The intrahepatic amount of TG was 2.5–3 \times higher in HcB19 mice than in C3H mice ($71 \pm 31 \mu\text{mol TG/mg}$ protein in C3H vs. 198 ± 92 in HcB19, $P < 0.01$, $n = 8$). Hepatic TG content correlated with fasting plasma concentrations of TG ($r = 0.632$, $P < 0.01$, Fig. 1A) and NEFA ($r = 0.525$, $P < 0.05$, Fig. 1B) but not with any other plasma parameter. Fatty liver was slightly more pronounced in female mice (hepatic TG content was $82 \pm 42 \mu\text{mol}$

TABLE 1. Fasting plasma parameters

	C3H	HcB19
Sex (M/F)	18/14	21/13
Age (weeks)	54 ± 15	57 ± 15
Weight (g)	22.3 ± 3.9	22.5 ± 4.5
TG (mM)	0.9 ± 0.3	$3.3 \pm 1.9^{**}$
Cholesterol (mM)	2.9 ± 0.6	$3.7 \pm 1.3^*$
Free fatty acids (mM)	0.54 ± 0.11	$0.69 \pm 0.19^{***}$

TG, Triglycerides.

* $P < 0.05$.

** $P < 0.005$.

*** $P < 0.001$.

TG/mg protein in C3H and 216 ± 92 in HcB19, $P < 0.05$, $n = 4$) than in male mice ($60 \pm 11 \mu\text{mol TG/mg}$ protein in C3H and 162 ± 98 in HcB19, $P = 0.085$, $n = 4$). Hepatic $\text{Fe}^{2+/3+}$ concentration was 3- to 4-fold higher in C3H mice than in HcB19 mice ($6.72 \pm 1.71 \mu\text{g/mg}$ liver protein, $n = 6$, vs. 1.79 ± 0.79 , $n = 6$; $P < 0.001$).

Proteome analysis

Fig. 2 shows representative examples of 2D gels from HcB19 and C3H liver homogenates, on which the differential spots are indicated. An average of 700–1,400 spots were visualized in the area included in the analyses. Eighteen protein spots were differential at the $P < 0.05$ level, and 11 of those were successfully identified on MALDI-TOF (Table 2). Among these were four novel proteins that were not previously identified in the differential pro-

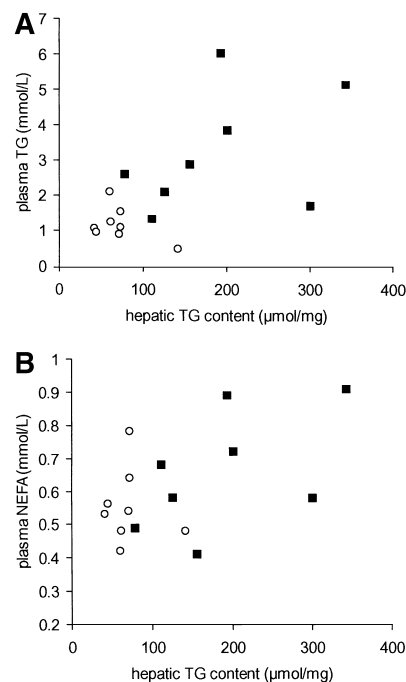


Fig. 1. Relationship between hepatic triglyceride (TG) content and plasma lipid parameters. C3H mice are represented by open circles and HcB19 mice by black squares. A: Correlation between plasma TG concentration and hepatic TG content is $r = 0.632$ ($P < 0.01$). B: Correlation between plasma NEFA concentration and hepatic TG content is $r = 0.525$ ($P < 0.05$).

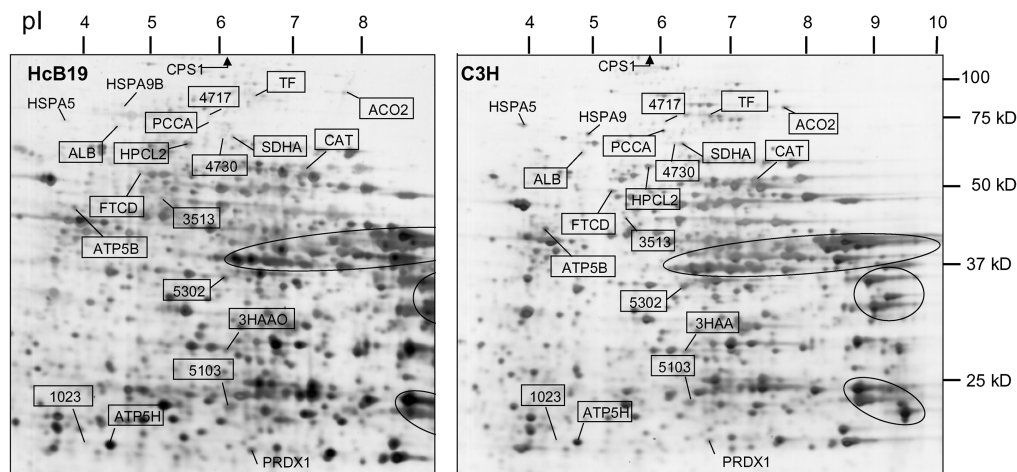


Fig. 2. Representative example of silver-stained 2D gels from HcB19 (left-hand panel) and C3H (right-hand panel). The differential proteins $P < 0.05$ are boxed. When identification was not successful, spots are indicated by their standard spot number. The ellipses indicate the areas of the images that were not analyzed for reasons of insufficient resolution. The positions of the molecular weight markers are indicated at the right-hand side.

teome of fatty livers [SDH subunit A (SDHA), aconitase (ACO2), propionyl CoA carboxylase α chain (PCCA), 3-hydroxyanthranilate 3,4 dioxygenase (3HAAO); $P < 0.05$]. Five differential proteins were mitochondrial [SDHA, ATP synthase β chain (ATP5B), ATP synthase D chain, ACO2, PCCA], two were peroxisomal [catalase (CAT), 2 hydroxy phytanol CoA lyase (HPCL2)], two were cytoplasmic [3HAAO, formiminotransferase cyclodeaminase (FTCD)], and two were secreted proteins [albumin (ALB), transferrin (TF)]. Proteins that were different at the $0.05 < P < 0.1$ level were also analyzed by MALDI-TOF, and four out of seven were identified [carbamoyl-phosphate synthase 1 (CPS1), PRDX1, glucose-regulated

78 kDa protein (HSPA5), heat shock 70 kDa protein 9; Table 2].

Confirmation of results

CAT and SDHA were quantified in the liver homogenates of HcB19 mice and C3H mice by immunoblotting (Fig. 3). The results confirmed that the amount of both CAT and SDHA protein was significantly reduced in livers of HcB19 mice compared with C3H mice. Expression of CAT in HcB19 expression was $73 \pm 5\%$ of expression in C3H ($P < 0.005$), and SDHA expression was $68\% \pm 14\%$ ($P = 0.006$ vs. C3H). Differential expression of PRDX was confirmed by RT-PCR. PRDX was of interest because this

TABLE 2. A short description of the protein identified in the MALDI analyses^a

Name	Function	Cellular Localization	Ratio HcB/C3H	P
SDHA	TCA cycle/respiratory chain (complex II)	Mitochondrial	0.21	0.001
ATP5B	Part of H(+) transporting ATPase	Mitochondrial	0.53	0.02
ACO2	TCA cycle	Mitochondrial	0.38	0.03
PCCA	Conversion of propionyl-CoA to succinyl-CoA; knock-out mice show fatty liver and increased ketone bodies	Mitochondrial	0.38	0.02
ATP5H	Part of H(+) transporting ATPase	Mitochondrial	1.59	0.02
CAT	H ₂ O ₂ removal	Peroxisomal	0.56	0.01
HPCL2	α -oxidation of three branched fatty acids	Peroxisomal	0.59	0.05
3HAAO	Conversion of 3 hydroxy anthranilate; final product = nicotinic acid	Cytoplasmic	0.38	0.01
FTCD	Channels 1-carbon units into the liver folate pool	Cytoplasmic	0.45	0.05
ALB	Plasma protein; among others transport of fatty acids	Secreted	0.53	0.02
TF	Transport of iron between tissues	Secreted	0.26	0.003
CPS1	Involved in urea cycle	Mitochondrial	0.54	0.1 (ns)
HSPA9B	HsP 70 kDa protein (Mortalin)	Cytoplasmic	0.42	0.07 (ns)
PRDX1	Reduces peroxides with reducing equivalents from the TRX system	Cytoplasmic	2.08	0.07 (ns) ^b
HSPA5 (BiP)	ER chaperone	ER lumen	0.53	0.07 (ns)

3HAAO, 3-hydroxyanthranilate 3,4 dioxygenase; ACO2, aconitase; ALB, albumin; ATP5B, ATP synthase β chain; ATP5H, ATP synthase D chain; BiP, binding protein; CAT, catalase; CPS1, carbamoyl-phosphate synthase 1; ER, endoplasmic reticulum; FTCD, formiminotransferase cyclodeaminase; HPCL2, 2 hydroxy phytanol CoA lyase; HSPA5, glucose-regulated 78 kDa protein; HSPA9, heat shock protein 70 kDa protein 9; MALDI, matrix-assisted laser desorption/ionization; ns, not significant; PCCA, propionyl CoA carboxylase α chain; PRDX, peroxiredoxin; SDHA, succinate dehydrogenase subunit A; TCA, trichloroacetic acid; TF, transferrin; TRX, thioredoxin.

^a Eleven out of 18 significant ($P < 0.05$) proteins and four out of seven proteins with $0.05 < P < 0.1$ were identified in the MALDI analyses.

^b Significant differential expression of peroxiredoxin 1 was shown using RT-PCR (see also Fig. 3).

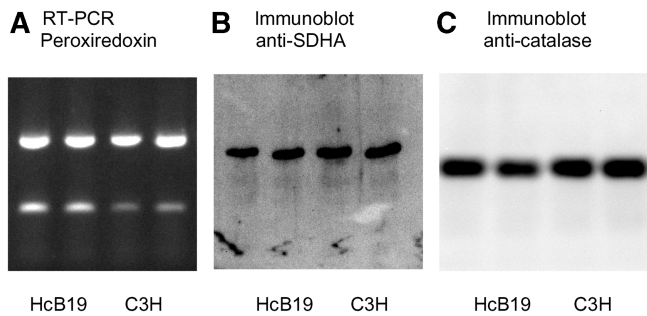


Fig. 3. Confirmation of 2D results and matrix-assisted laser desorption/ionization identification. The results of three of the identified proteins were confirmed using independent biochemical methods. Representative examples of the results of these assays are presented in A–C. Lanes 1 and 2 are duplicate results for HcB19 samples, and lanes 3 and 4 are duplicate results for C3H samples. A: PCR products of the duplex RT-PCR performed on RNA isolated from snap-frozen mouse liver tissue were separated on a 1.5% agarose gel and stained with ethidium bromide. Equal amounts of total RNA were used in the RT-PCR reactions. PCR products were quantified using the Quantity One program and data were expressed as the ratio of peroxiredoxin 1 (upper band)/ β -actin (lower band). B, C: Immunoblots of whole-mouse liver homogenate. Equal amounts of total liver proteins were separated on 7.5% SDS-PAGE and blotted onto polyvinylidene difluoride membranes. Membranes were probed with anti-succinate dehydrogenase (70 kDa) (B) or with anticatalase (60 kDa) (C) and the appropriate second antibody visualized with chemoluminescence and quantified using the Quantity One program.

enzyme uses reducing equivalents provided through the TRX system to reduce peroxides. Quantification of PDRX1 mRNA confirmed that PRDX1 expression, which tended to be higher in HcB19 liver homogenates than in C3H liver homogenates on the 2D gels ($P = 0.07$), was indeed different between the two mouse strains. The ratio of PRDX1 to β -actin expression in HcB19 mice (1.86 ± 0.27) was 1.6-fold higher than in C3H mice (1.14 ± 0.09 ; $P = 0.001$).

DISCUSSION

HcB19 mice are an inbred mouse strain in which TXNIP, a cytoplasmic inhibitor of TRX, is truncated (13). Absence of functional TXNIP, as in HcB19, could abolish TRX inhibition and increase the reducing capacity of the TRX/TRX reductase system (19). Indeed, we show here that PRDX, which uses reducing equivalents provided by the TRX/TRX reductase system, is expressed at significantly higher levels in HcB19 mice. This suggested that the TRX system is more active in the delivery of reducing equivalents to PRDX1 in HcB19 mice than in C3H mice, and indicates a shift of antioxidant activity toward the TRX/TRX reductase system in the livers of HcB19 mice. Recently, Simuda et al. (20) reported that patients with NASH had elevated plasma levels of TRX, suggesting that TRX levels reflect progression from fatty liver (steatosis) to steatohepatitis. Combined, the presented data and those reported (20) should stimulate further research into the role of the TRX/TRX reductase and the TXNIP regulatory system in NASH.

At present, only a limited number of studies addressing protein expression in hepatic steatosis or NASH have been published (9–11). The present data identified several proteins that have been implicated in steatosis or NASH in the literature: ATP5B, ALB, FTCD, HPCL2, CAT, HSPA5, and CPS1. This confirmation is of significant interest because the animals used in the previous studies had different genetic backgrounds than the steatotic HcB19 mice used in the present analyses, so apparently these proteins reflect general mechanisms in steatosis.

Four out of 11 proteins in the differential proteome have previously been associated with intracellular iron (TF; ACO2; SDH; 3HAAO, 3 hydroxyanthranilate 3,4 dioxygenase). Notably, TRX modulates activity of iron regulatory proteins by altering their binding to RNA (21), and it is likely that absence of functional TXNIP increased TRX activity in HcB19 mice. Lower levels of ACO2 and SDHA in HcB19 (ratios of HcB19 over C3H were 0.38 and 0.21, respectively) can indicate lower intracellular iron concentrations [as reviewed in ref. (22)], and indeed we measured a highly significant, 3- to 4-fold, lower iron concentration in HcB19 livers than in C3H livers. Apparently, HcB19 mice can develop fatty liver without increased hepatic iron concentrations, which is interesting in the light of the ongoing debate on the role of hepatic iron in the development of steatosis and nonalcoholic fatty liver disease (20, 23, 24). Several explanations may be possible for the observed relationship between lower hepatic iron content and the presence of steatosis other than TXNIP deficiency. One alternative explanation is that C3H, the parental strain of the inbred HcB19 mice, has a spontaneous mutation in an additional gene that affects hepatic iron stores (A. J. Lusis, UCLA, personal communication). On the other hand, our own preliminary data in a human population study suggest that female carriers of the rare allele of a single nucleotide polymorphism in TXNIP have significantly higher plasma iron concentrations and lower unbound-iron binding capacity, as well as increased iron-saturation, than carriers of the common allele (M. M. J. van Greevenbroek et al., unpublished observations). In HcB19 mice, low hepatic iron stores and differential expression of several proteins associated with iron metabolism (TF, ACO2, SDHA, 3HAAO) can, therefore, at least partly, result from the absence of full-length TXNIP in HcB19 mice.

Four new differential proteins were identified: SDHA, ACO2, PCCA, and 3HAAO. SDHA and ACO2 have not been implicated in fatty liver before, and deficiencies in these genes have been associated with neurodegenerative disorders and myopathies (25, 26). Nevertheless, the lower expression of these two enzymes is in agreement with the reduced tricarboxylic acid cycle activity that was demonstrated in the livers of HcB19 mice (13). Several of the novel hepatic proteins that we identified as differential in steatosis may be functionally involved in the development of fatty liver. PCCA is a biotin-dependent enzyme that catalyses the first of three steps in the conversion of propionyl-CoA to succinyl-CoA, which will subsequently enter the citric acid cycle. PCCA is the key enzyme in the

catabolic pathway of odd-chain fatty acids, isoleucine, threonine, methionine, and valine. It has been shown that PCCA^{-/-} mice exhibit fatal extreme ketoacidosis as well as fatty liver (27). In the present study, HcB19 mice had significantly lower levels of PCCA than C3H mice (ratio 0.38). Low levels of PCCA in the livers of HcB19 mice can help explain the increased levels of ketone bodies reported in HcB19 mice (13). A possible mechanism involves the common transcription factor AP-1. Abdullah et al. (28) showed binding of fatty acids to AP-1 (*c-jun*), which resulted in suppression of the expression of CPS1. Altered transcription can also occur in other genes that have a similar (putative) AP-1 enhancer site, such as ALB (29) and PCCA (30), and may be a generalized mechanism relevant to the development of fatty liver. Of note, CPS-1, ALB, and PCCA were all lower in HcB19 mice (Table 2). AP-1 is a redox-sensitive transcription factor (31), and this can be relevant in the light of the primary TXNIP gene defect and a possibly altered redox state in HcB19 mice.

With regard to the hypertriglyceridemia in HcB19 mice, 3HAAO is a promising conceptual candidate. 3HAAO is involved in tryptophan catabolism, converting 3-hydroxyanthranilate and dioxigen into a precursor that spontaneously converts to quinolinic acid and, subsequently, to nicotinic acid. Niacin (nicotinic acid) has been shown to decrease the hepatic VLDL TG production rate in healthy human subjects (32), and a 2-fold reduction of 3HAAO has been reported in the liver of hypercholesterolemic rabbits (33). Additionally, several clinical studies have shown that niacin treatment in (familial) combined hyperlipidemia primarily improves the TG and HDL status (34, 35). Recently, we found that FCHL subjects with fatty liver have hypertriglyceridemia or combined hyperlipidemia (4). Thus, the lower 3HAAO levels we found in HcB19 livers may contribute to the hypersecretion of VLDL that has been reported in HcB19 mice (12).

In conclusion, in a comprehensive analysis of the hepatic proteins of HcB19 mice with fatty liver, we have identified several novel differential proteins, including PCCA and 3HAAO, compared with the parental strain. Both proteins are strong conceptual candidates for the molecular pathogenesis of fatty liver with hyperlipidemia. Future experiments using TXNIP-deficient mice in a presteatotic stage may reveal which of these proteins are causal in hepatic TG accumulation. 

The authors thank F. Bouwman of the Maastricht University Proteomics Center (Dr. E. Mariman, Head) for doing the matrix-assisted laser desorption/ionization-time of flight analyses, Dr. P. Demant for providing the authors with the HcB19 and C3H mouse strains, Dr. J. Bodnar for advice on the HcB19 genotyping, Dr. L. Nijmans for help with the succinate dehydrogenase subunit A immunoblots, and Dr. A. J. Lusis for critical discussions.

REFERENCES

- Pessayre, D., A. Berson, B. Fromenty, and A. Mansouri. 2001. Mitochondria in steatohepatitis. *Semin. Liver Dis.* **21**: 57–69.
- Schonfeld, G., B. W. Patterson, D. A. Yablonskiy, T. S. Tanoli, M. Averna, N. Elias, P. Yue, and J. Ackerman. 2003. Fatty liver in familial hypobetalipoproteinemia: triglyceride assembly into VLDL particles is affected by the extent of hepatic steatosis. *J. Lipid Res.* **44**: 470–478.
- den Boer, M., P. J. Voshol, F. Kuipers, L. M. Havekes, and J. A. Romijn. 2004. Hepatic steatosis: a mediator of the metabolic syndrome: lessons from animal models. *Arterioscler. Thromb. Vasc. Biol.* **24**: 1–6.
- T. W. A. de Bruin, A. M. Georgieva, M. C. G. J. Brouwers, M. V. Heitink, C. J. H. van der Kallen, and M. M. J. van Greevenbroek. 2004. Radiological evidence of nonalcoholic fatty liver disease in familial combined hyperlipidemia. *Am. J. Med.* In press.
- Lewis, G. F., A. Carpentier, K. Adeli, and A. Giacca. 2002. Disordered fat storage and mobilization in the pathogenesis of insulin resistance and type 2 diabetes. *Endocr. Rev.* **2**: 201–229.
- Caldwell, S. H., D. H. Oelsner, J. C. Tezzoni, E. E. Hespdenheide, E. H. Battle, and C. J. Driscoll. 1999. Cryptogenic cirrhosis: clinical characterization and risk factors for underlying disease. *Hepatology.* **29**: 664–669.
- Lee, R. G. 1989. Nonalcoholic steatohepatitis: a study of 49 patients. *Hum. Pathol.* **20**: 594–598.
- Chitturi, S., and J. George. 2003. Interaction of iron, insulin resistance, and nonalcoholic steatohepatitis. *Curr. Gastroenterol. Rep.* **5**: 18–25.
- Santamaria, E., M. A. Avila, M. U. Latasa, A. Rubio, A. Martin-Duce, S. C. Lu, J. M. Mato, and F. J. Corrales. 2003. Functional proteomics of nonalcoholic steatohepatitis: mitochondrial proteins as targets of S-adenosylmethionine. *Proc. Natl. Acad. Sci. USA.* **100**: 3065–3070.
- Edvardsson, U., H. Brockenhuus Von Lowenhielm, O. Panfilov, A. C. Nystrom, F. Nilsson, and B. Dahllof. 2003. Hepatic protein expression of lean mice and obese diabetic mice treated with peroxisome proliferator-activated receptor activators. *Proteomics.* **3**: 468–478.
- Sanchez, J. C., V. Converset, A. Nolan, G. Schmid, S. Wang, M. Heller, M. V. Sennitt, D. F. Hochstrasser, and M. A. Cawthorne. 2003. Effect of rosiglitazone on the differential expression of obesity and insulin resistance associated proteins in *lep/lep* mice. *Proteomics.* **3**: 1500–1520.
- Castellani, L. W., A. Weinreb, J. Bodnar, A. M. Goto, M. Doolittle, M. Mehrabian, P. Demant, and A. J. Lusis. 1998. Mapping a gene for combined hyperlipidaemia in a mutant mouse strain. *Nat. Genet.* **18**: 374–377.
- Bodnar, J. S., A. Chatterjee, L. W. Castellani, D. A. Ross, J. Ohmen, J. Cavalcoli, C. Wu, K. M. Dains, J. Catanese, M. Chu, S. S. Sheth, K. Charugundla, P. Demant, D. B. West, P. de Jong, and A. J. Lusis. 2003. Positional cloning of the combined hyperlipidemia gene *Hyp1p1*. *Nat. Genet.* **30**: 110–116.
- Pajukanta, P., I. Nuotio, J. D. Terwilliger, K. V. Porkka, K. Ylitalo, J. Pihlajamaki, A. J. Suomalainen, A. C. Syvanen, T. Lehtimaki, J. S. Viikari, M. Laakso, M. R. Taskinen, C. Ehnholm, and L. Peltonen. 1998. Linkage of familial combined hyperlipidaemia to chromosome 1q21-q23. *Nat. Genet.* **18**: 369–373.
- Pei, W., H. Baron, B. Muller-Myhok, H. Knoblauch, S. A. Al-Yahyaee, R. Hui, X. Wu, L. Liu, A. Busjahn, F. C. Luft, and H. Schuster. 2000. Support for linkage of familial combined hyperlipidemia to chromosome 1q21-q23 in Chinese and German families. *Clin. Genet.* **57**: 29–34.
- Coon, H., R. H. Myers, I. B. Borecki, D. K. Arnett, S. C. Hunt, M. A. Province, L. Djousse, and M. F. Leppert. 2000. Replication of linkage of familial combined hyperlipidemia to chromosome 1q with additional heterogeneous effect of apolipoprotein A-I/C-III/A-IV locus. The NHLBI Family Heart Study. *Arterioscler. Thromb. Vasc. Biol.* **20**: 2275–2280.
- van Deursen, C., M. de Metz, J. Koudstaal, and P. Brombacher. 1988. Accumulation of iron and iron compounds in liver tissue. A comparative study of the histological and chemical estimation of liver iron. *J. Clin. Chem. Clin. Biochem.* **26**: 617–622.
- Shevchenko, A., M. Wilm, O. Vorm, and M. Mann. 1996. Mass spectrometric sequencing of proteins from silverstained polyacrylamide gels. *Anal. Chem.* **68**: 850–858.
- Nordberg, J., and E. S. Arner. 2001. Reactive oxygen species, antioxidants, and the mammalian thioredoxin system. *Free Radic. Biol. Med.* **31**: 1287–1312.
- Sumida, Y., T. Nakashima, T. Yoh, M. Furutani, A. Hirohama, Y. Kakisaka, Y. Nakajima, H. Ishikawa, H. Mitsuyoshi, T. Okanoue, K.

- Kashima, H. Nakamura, and J. Yodoi. 2003. Serum thioredoxin levels as a predictor of steatohepatitis in patients with nonalcoholic fatty liver disease. *J. Hepatol.* **38**: 32–38.
21. Oliveira, L., C. Bouton, and J. C. Drapier. 1999. Thioredoxin activation of iron regulatory proteins. Redox regulation of RNA binding after exposure to nitric oxide. *J. Biol. Chem.* **274**: 516–521.
22. Templeton, D. M., and Y. Liu. 2003. Genetic regulation of cell function in response to iron overload or chelation. *Biochim. Biophys. Acta.* **1619**: 113–124.
23. Agrawas, S., and H. L. Bonkovsky. 2002. Management of steatohepatitis: an analytical review. *J. Clin. Gastroenterol.* **35**: 253–261.
24. Washington, K., K. Wright, Y. Shyr, E. B. Hunter, S. Olson, and D. S. Raiford. 2000. Hepatic stellate activation in non-alcoholic steatohepatitis and fatty liver. *Hum. Pathol.* **31**: 822–828.
25. Baysal, B., W. Rubinstein, and P. Taschner. 2001. Phenotypic dichotomy in mitochondrial complex II genetic disorders. *J. Mol. Med.* **79**: 495–503.
26. Drugge, U., M. Holmberg, G. Holmgren, B. Almay, and H. Linderholm. 1995. Hereditary myopathy with lactic acidosis, succinate dehydrogenase and aconitase deficiency in northern Sweden. *J. Med. Genet.* **32**: 344–347.
27. Miyazaki, T., T. Ohura, M. Kobayashi, Y. Shigematsu, S. Yamaguchi, Y. Suzuki, I. Hata, Y. Aoki, X. Yang, C. Minjares, I. Haruta, H. Uto, Y. Ito, and U. Muller. 2001. Fatal propionic acidemia in mice lacking propionyl-CoA carboxylase and its rescue by postnatal, liver-specific supplementation via a transgene. *J. Biol. Chem.* **276**: 35995–35999.
28. Abdullah Abu Musa, D. M., K. Kobayashi, I. Yasuda, M. Iijima, V. M. Christoffels, M. Tomomura, M. Horiuchi, T. Ohnishi, T. Kajihara, Y. Daikuhara, W. H. Lamers, and T. Saheki. 1999. Involvement of a cis-acting element in the suppression of carbamoyl phosphate synthetase I gene expression in the liver of carnitine-deficient mice. *Mol. Genet. Metab.* **68**: 346–356.
29. Hu, J., and H. C. Isom. 1994. Suppression of albumin enhancer activity by H-ras and AP-1 in hepatocyte cell lines. *Mol. Cell. Biol.* **14**: 1531–1543.
30. Campeau, E., L. R. Desviat, D. Leclerc, X. Wu, B. Perez, M. Ugarte, and R. A. Gravel. 2001. Structure of the PCCA gene and distribution of mutations causing propionic acidemia. *Mol. Genet. Metab.* **74**: 238–247.
31. Karimpour, S., J. Lou, L. L. Lin, L. M. Rene, L. Lagunas, X. Ma, S. Karra, C. M. Bradbury, S. Markovina, P. C. Goswami, K. Hirota, D. V. Kalvakolanu, J. Yodoi, and D. Gius. 2002. Thioredoxin reductase regulates AP-1 activity as well as thioredoxin nuclear localization via active cysteines in response to ionizing radiation. *Oncogene.* **21**: 6317–6327.
32. Wang, W., A. Basinger, R. A. Neese, B. Shane, S. A. Myong, M. Christiansen, and M. K. Hellerstein. 2001. Effect of nicotinic acid administration on hepatic very low density lipoprotein-triglyceride production. *Am. J. Physiol. Endocrinol. Metab.* **280**: E540–E547.
33. Ragazzi, E., C. V. Costa, L. Caparrotta, M. Biasiolo, A. Bertazzo, and G. Allegri. 2002. Enzyme activities along the tryptophan-nicotinic acid pathway in alloxan diabetic rabbits. *Biochim. Biophys. Acta.* **1571**: 9–17.
34. McKenney, J. M., L. S. McCormick, S. Weiss, M. Koren, S. Kafonek, and D. M. Black. 1998. A randomized trial of the effects of atorvastatin and niacin in patients with combined hyperlipidemia or isolated hypertriglyceridemia. Collaborative Atorvastatin Study Group. *Am. J. Med.* **104**: 137–143.
35. Mostaza, J. M., I. Schulz, G. L. Vega, and S. M. Grundy. 1997. Comparison of pravastatin with crystalline nicotinic acid monotherapy in treatment of combined hyperlipidemia. *Am. J. Cardiol.* **79**: 1298–1301.